

DGP-LVM: Derivative Gaussian process latent variable models

Soham Mukherjee^{1,2,3}, Manfred Claassen^{2,3}, and Paul-Christian Bürkner¹

¹*Department of Statistics, Technical University of Dortmund, Dortmund, Germany*

²*Department of Computer Science, University of Tübingen, Tübingen, Germany*

³*University Hospital Tübingen, Faculty of Medicine, University of Tübingen, Tübingen, Germany*

Abstract

We develop a framework for derivative Gaussian process latent variable models (DGP-LVM) that can handle multi-dimensional output data using modified derivative covariance functions. The modifications account for complexities in the underlying data generating process such as scaled derivatives, varying information across multiple output dimensions as well as interactions between outputs. Further, our framework provides uncertainty estimates for each latent variable samples using Bayesian inference. Through extensive simulations, we demonstrate that latent variable estimation accuracy can be drastically increased by including derivative information due to our proposed covariance function modifications. The developments are motivated by a concrete biological research problem involving the estimation of the unobserved cellular ordering from single-cell RNA (scRNA) sequencing data for gene expression and its corresponding derivative information known as RNA velocity. Since the RNA velocity is only an estimate of the exact derivative information, the derivative covariance functions need to account for potential scale differences. In a real-world case study, we illustrate the application of DGP-LVMs to such scRNA sequencing data. While motivated by this biological problem, our framework is generally applicable to all kinds of latent variable estimation problems involving derivative information irrespective of the field of study.

Keywords: Gaussian processes, single-cell RNA, Bayesian inference, derivatives, latent variables

1 Introduction

Gaussian processes (GPs) are a class of statistical models known for their flexible structure and favourable properties to analyze complex data (Williams and Rasmussen, 1995). Since their inception, several extensions have been proposed, among which the most relevant ones to this paper are adding derivative information to GPs (Solak et al., 2002; Rasmussen and Williams, 2006), building GPs with multiple outputs (Cressie, 1993; Teh et al., 2005; Rasmussen and Williams, 2006) as well as modeling latent input variables (Lawrence, 2003, 2005). Since differentiation is a linear operation, any variable and its derivative would be linearly related. For the same reason, as a fundamental property of GPs, a derivative of a GP is just another GP with a related covariance function. Together, this results in a single GP model for the outputs and their derivatives with a joint derivative covariance function (Solak et al., 2002).

Derivative GPs have usually been studied and designed to model a single vector-valued output and have not been extended for multiple outputs. Multi-output GPs are most suitable when the response or output of the model contains multiple features, each expressed by its own dimension. One could fit individual GPs for each feature but then risks substantial loss of information in case of interactions between features. Thus a two-fold covariance structure was suggested in (Teh et al., 2005) allowing GPs to account for this shared information between features. We extend this two-fold covariance structure to derivative GPs. As we will motivate more in a bit,

our primary aim is to estimate latent (input) variables from observed input variables measured with error and output variables connected to the inputs via GPs; a challenge leading to what are called latent GPs (Lawrence, 2003). When using derivative GPs, such latent inputs are shared between the original outputs and their derivative counterparts, effectively doubling the amount of information available for estimating the latent inputs.

In real-world data, the derivatives are seldom exactly computed, which adds a major challenge to the modeling endeavour. If derivatives are computed with respect to the observed (non-latent) inputs, they are naturally only an approximation of the derivatives with respect to latent inputs. Conversely, if the derivatives are (implicitly) computed with respect to the latent inputs, the uncertainty of the latter will induce hard-to-quantify uncertainty in the estimated derivatives. One way or another, this lack of exact derivative information poses a serious challenge for derivative GP modeling. Existing approaches are not equipped to deal with the significant scale differences between outputs and derivatives, thus requiring modifications in its covariance functions to ensure valid and efficient latent variable estimation.

In this paper, we demonstrate a combination of all the above model extensions leading to our DGP-LVM: derivative Gaussian process latent variable model framework. We provide more context about the real-world modeling challenges in Section 1.1 as a basis for our motivation to develop DGP-LVM. The remainder of the paper is structured as follows. We discuss and provide context on related works in Section 2. We introduce our methodology and model development in Section 3 and perform extensive simulation studies in Section 4 that demonstrate the relevance of our contributions. We further illustrate DGP-LVM on a real single-cell RNA sequencing data in Section 5 before discussing our methods’ limitations and future work in Section 6.

1.1 Motivation

In developmental biology, to describe temporal biological processes, researchers use stochastic approaches to understand cellular progression, that is, how cells develop and undergo changes in their state throughout various stages over the period of time (Maamar et al., 2007; Losick and Desplan, 2008; Raj and Oudenaarden, 2008). Currently, this problem is frequently tackled with single-cell RNA sequencing (scRNA-seq) technologies by analysing messenger-RNA (mRNA) molecule counts as a measure of gene expression (Haque et al., 2017). The measured gene expression (also called expression levels) provide the necessary information about the nature of cells at a specific point of time, also known as cell states, as well as their changes over time. However, due to the experimental limitations of the current sequencing methods each cell gets destroyed in the measurement process and can therefore be observed only once. This situation makes it difficult to infer cell state transitions and the overall sequence of cell states of a temporal biological process. To that end, pseudotime ordering is a popular approach to describe such a biological process as a sequence of cell states along a time sequence. (Trapnell et al., 2014).

Single-cell gene expression data provides information about cell state snapshots. While conventional pseudotime ordering approaches operate only on cell state snapshots to estimate pseudotime, only recently, directional information about cell state changes (i.e., derivative information) has been accounted for in this task (Gupta et al., 2022). Here, we hypothesise and demonstrate empirically later that including directional information on cell state transitions increases the precision in estimating pseudotime. This directional information is available through a quantity known as RNA velocity that is estimated from the difference in unspliced and spliced gene expression levels over latent experimental time (not to be confused with pseudotime) (La Manno et al., 2018; Bergen et al., 2020). By construction, this RNA velocity estimates the derivative of spliced gene expression data with respect to time. Concretely, our aim is to enable using the combination of RNA gene expression and RNA velocity in a single probabilistic framework for

pseudotime estimation. This combination of RNA gene expression and its corresponding RNA velocity requires a novel statistical model approach.

In order to model such data, certain requirements must be satisfied. Starting from support for multi-dimensional outputs that allows inclusion of several genes for each cell, the model should account for varying gene-specific information as well as possible biologically induced interactions among genes. Moreover, since RNA velocity is only a derivative *estimation* of gene expression levels, they are frequently on a significantly different scale than the gene expression levels. Dealing with this scale difference is a challenge that the model must address in order to provide reliable pseudotime estimates. In this paper, we demonstrate that DGP-LVM is able to tackle all of the above challenges and can estimate latent input variables with significantly higher accuracy than other GP models. Thus, we also demonstrate its potential to be applicable to estimating pseudotime through RNA gene expressions and their corresponding RNA velocities.

1.2 Contributions

- We develop a probabilistic GP modeling framework for latent (input) variable estimation using derivative information for any multi-dimensional data-generating process. Our model accounts for dimension specific information and interactions between dimensions in a multi-dimensional data scenario which are common in fields like single-cell biology.
- We develop a custom derivative structure for Squared Exponential (SE) and Matern class of covariance functions that is able to account for significant scale differences between the outputs and its corresponding derivatives.
- Through extensive simulations, we demonstrate that our model provides substantially more accurate latent variable estimates than other GP models under realistic scenarios.
- We showcase the application of our modeling approach on a reduced real-world scRNA data set.

2 Related work

Gaussian processes, as a class of models, underwent a wide range of extensions over the years giving rise to various forms of GP models. Specifically, three broad extensions relevant to this work are GPs with derivative information, multi-output GPs and GPs for latent variable modeling. Using derivative information for Gaussian processes was introduced in Solak et al. (2002) who replaced standard covariance functions with their derivative counterparts. This paved the way to modeling data along with its derivatives as a single GP model. Recently, derivative GPs were extended to support multiple inputs and scalable approximations (Eriksson et al., 2018; Padidar et al., 2021). In case of multi-output GPs, recent works (Moreno-Muñoz et al., 2018; Joukov and Kulić, 2022) study GPs with support for multiple outputs that are of varying nature in terms of data types, however multi-output GPs with derivative information have not been studied in detail yet. Latent GPs were introduced by Lawrence (2003, 2005) and have, so far, been predominantly used for dimensionality reduction (Titsias, 2009; Titsias and Lawrence, 2010). More recently, for similar applications of dimension-reduction technique, extensions on GP latent variable model for non-Gaussian likelihoods with different types of latent input structures were discussed in Lalchand et al. (2022). These works also focus on scalable approximations to latent GPs. In contrast, we focus estimating latent inputs that probabilistically explains a dependent multi-output variable.

For the modeling of scRNA sequencing data, GPs have been broadly applied in two relevant directions, specifically, for clustering (Buettner and Theis, 2012; Buettner et al., 2015) and temporal modeling (Hensman et al., 2013b). Considering the latter, pseudotime estimation

constitutes a major research direction as it is directly related to understanding the true underlying biological processes. It has been shown previously that point estimates of pseudotime are highly prone to infer false cellular ordering, thus suggesting Bayesian inference to provide uncertainty estimates alongside each estimated pseudotime (Campbell and Yau, 2015). Further works focus on latent pseudotime estimations (Reid and Wernisch, 2016; Campbell and Yau, 2018) along with branching structures for trajectory inference (Ahmed et al., 2019) based on a GP framework. One of the main limitations in these works lies in their restricted use of gene expressions, taking into account expression profile snapshots as the only available information regarding cellular ordering. We provide evidence that including RNA velocity as derivative information holds the power to estimate latent pseudotime with increased precision compared to what previous approaches could achieve.

3 Methods

We develop DGP-LVM, a framework for derivative Gaussian process modeling with the primary goal of estimating latent variables serving as (implicit) inputs to the GP. As the general setup, we consider a pair of variables (y, x) where y is the output (response) variable and x is the input variable (covariate), with individual observations denoted as $y_i, x_i \in \mathbb{R}, i = \{1, \dots, N\}$ where N is the number of observations. In addition to y itself, we incorporate the derivative outputs $y' = \delta y / \delta x$ into the model. The components of DGP-LVM are first discussed individually, before we combine them into a single model.

3.1 Derivative Gaussian processes

A GP is a stochastic process specified by a mean function $m(x)$ (usually fixed to zero), and a covariance function $K = K(x, x^T)$, where x^T indicate transpose of x , such that a finite set of these points will follow a multivariate Gaussian distribution (Williams and Rasmussen, 1995). Here, we consider zero-mean GPs $f(x)$ such that $f(x) \sim \mathcal{GP}(0, K)$. If the output variable y is univariate, modeling the relationship of x and y via a (single-output) GP and independent additive noise can be written as

$$y_i = f(x_i) + \varepsilon_i, \quad (1)$$

where ε_i is the i^{th} sample of $\varepsilon \sim \mathcal{N}(0, \sigma^2)$ assuming equal-variance Gaussian noise. Together, this is equivalent to

$$y_i \sim \mathcal{N}(f(x_i), \sigma^2). \quad (2)$$

For, $i \neq j$ we have $\text{Cov}(y_i, y_j) = K(x_i, x_j)$ and for $i = j$, we have $\text{Cov}(y_i, y_j) = \text{Var}(y_i) = K(x_i, x_j) + \sigma^2$. The above notation will be extended to multi-output GPs in Section 3.2.

GPs are able to take advantage of derivatives in addition to its corresponding sample data to increase model accuracy. Since differentiation is a linear operator, a derivative of a GP is just another GP (Solak et al., 2002; Rasmussen and Williams, 2006). This property of GPs can be utilised to take derivative of a joint covariance structure of both y and y' , if the second order derivative of the covariance function exists. The (joint) derivative GP is then given by

$$\begin{pmatrix} f(x) \\ f'(x) \end{pmatrix} \sim \mathcal{GP} \left(0, \begin{pmatrix} K & K' \\ K'^T & K'' \end{pmatrix} \right), \quad (3)$$

where K' is the first derivative of the covariance function $K = K(x, x^T)$ with respect to x and K'^T is the first derivative of the covariance function with respect to x^T . K'' is the second order partial derivative of K differentiating both with respect to x and x^T . In other words, differentiation simply propagates through the covariance function (see Appendix A for mathematical details). The specific properties of such derivative GP models depend on the chosen covariance

function. A common choice is the Squared Exponential (SE) covariance function with hyperparameters ρ as length scale and α as the GP marginal standard deviation (SD). The derivative version of the SE covariance function is given by

$$K(x_i, x_j) = \alpha^2 \exp\left(-\frac{(x_i - x_j)^2}{2\rho^2}\right), \quad (4)$$

$$K'(x_i, x_j) = \alpha^2 \frac{(x_i - x_j)}{\rho^2} \exp\left(-\frac{(x_i - x_j)^2}{2\rho^2}\right), \quad (5)$$

$$K''(x_i, x_j) = \frac{\alpha^2}{\rho^4} (\rho^2 - (x_i - x_j)^2) \exp\left(-\frac{(x_i - x_j)^2}{2\rho^2}\right). \quad (6)$$

Derivative covariance functions are obtainable generally for any chosen covariance function whose second order derivative exists. In this paper, we focus on SE and Matern class covariance functions as perhaps the most common choices. We provide derivative SE, Matern 3/2 and Matern 5/2 covariance functions in Appendix A. In our real-world case study (Section 5), we specifically consider the SE and Matern 3/2 as the extreme cases in terms of smoothness among the Matern class covariance functions.

3.1.1 Customised hyperparameters

Properly including the derivative observations y' requires more than just using a basic derivative covariance function. Due to the properties of differentiation, y' can be on a fundamentally different scale than y and thus, needs to be treated as such. In addition to having a different mean (i.e., different GP components $f(x)$ vs. $f'(x)$), the error SDs for y and y' will also be different. Moreover, for real data, the observations y' containing derivative information may not be the exact same as the true derivatives $\delta y/\delta x$, but only be proportional to them (see Section 1). This proportionality induces a scale difference between y' and what is canonically modeled by a basic derivative covariance function. This creates a major issue for models ignoring scale differences as we demonstrate in our simulations.

To incorporate these scale considerations into our model, we propose to adjust the covariance function hyperparameters. Again using the SE covariance function as an example, we propose to introduce a second marginal SD parameter α' , corresponding to the derivative part of the GP, while α now only concerns the original part of the GP:

$$K(x_i, x_j) = \alpha^2 \exp\left(-\frac{(x_i - x_j)^2}{2\rho^2}\right), \quad (7)$$

$$K'(x_i, x_j) = \alpha\alpha' \frac{(x_i - x_j)}{\rho^2} \exp\left(-\frac{(x_i - x_j)^2}{2\rho^2}\right), \quad (8)$$

$$K''(x_i, x_j) = \frac{\alpha'^2}{\rho^4} (\rho^2 - (x_i - x_j)^2) \exp\left(-\frac{(x_i - x_j)^2}{2\rho^2}\right). \quad (9)$$

We also introduce a second error SD parameter σ' corresponding only to the derivative outputs. We assume both the GP marginal SD and error SD parameters are related to each other, respectively, through scalar multiples due to scale difference between y and y' . The scale of ρ is only dependent on the scale of x , which is constant across outputs and their derivatives, such that ρ does not need to be split up into two parameters. Together, independent of specifically chosen covariance function, the DGP-LVM on y and y' with independent, additive Gaussian noise is then specified as

$$y_i \sim \mathcal{N}(f(x_i), \sigma^2) \quad \text{and} \quad y'_i \sim \mathcal{N}(f'(x_i), \sigma'^2). \quad (10)$$

3.2 Multidimensional outputs

Multivariate output GPs (or multi-output GPs) model multiple response variables $\{y_1, \dots, y_D\}$ jointly over $D > 1$ output dimensions (Rasmussen and Williams, 2006). Extending our univariate notation, the individual output values are now denoted as y_{di} for dimension d and observation i , with corresponding derivative values y'_{di} . Multi-output GPs are created by first setting up D independent, univariate Gaussian processes $f_d(x)$ each with their own set of hyperparameters, that is, $(\rho_d, \alpha_d, \alpha'_d, \sigma_d$ and $\sigma'_d)$ for Matern covariance functions with adjusted scales. Subsequently the univariate GPs are related to one another by folding them with a (D -dimensional) across-dimension correlation matrix C (Teh et al., 2005; Bonilla et al., 2007). That is, for each observation i , we obtain a vector of across-dimension correlated GP values as

$$\begin{pmatrix} \tilde{f}_1(x_i) \\ \dots \\ \tilde{f}_D(x_i) \end{pmatrix} = L \times \begin{pmatrix} f_1(x_i) \\ \dots \\ f_D(x_i) \end{pmatrix}, \quad (11)$$

where L is the Cholesky factor of C , that is, $C = LL^T$ with L being lower-triangular. This way, multi-output GPs combine two dependency structures, one within dimensions (and across observations) as expressed by the univariate GPs through corresponding covariance functions and one across output dimensions (but within observations) as expressed by C (or L).

This readily generalizes to derivative GPs by applying Equation (11) to the derivative GP values $f'_d(x_i)$ as well, which results in the across-dimension correlated values $\tilde{f}'_d(x_i)$. Adding independent Gaussian noise, our derivative multi-output GP model then implies for all d and i :

$$y_{di} \sim \mathcal{N}(\tilde{f}_d(x_i), \sigma_d^2) \quad \text{and} \quad y'_{di} \sim \mathcal{N}(\tilde{f}'_d(x_i), \sigma_d'^2). \quad (12)$$

3.3 Latent variable inputs

So far, we have considered the input x to be known exactly. However, in practice, we often only have a noisy measurement \tilde{x} of x available. In this context, the true x becomes a latent variable, which needs to be appropriately modeled and subsequently estimated. If we assume that the measurements \tilde{x} are Gaussian with known measurement SD s , we can write for each observation i :

$$\tilde{x}_i \sim \mathcal{N}(x_i, s^2). \quad (13)$$

The implied latent x_i is then passed to the GP covariance function, which results in what is known as latent(-input) GPs (Lawrence, 2003, 2005; Titsias and Lawrence, 2010). Such latent-input GPs are even harder to fit than their non-latent counterparts: Not only does the number of unknowns increase substantially, but also new identification issues arise due to both x and ρ now being unknown (see Section 3.4 for details on how we deal with this).

3.4 The full model

Combining all of the above model components results in our DGP-LVM framework. As such, DGP-LVM can be applied to the aforementioned problem of pseudotime estimation from single-cell RNA sequencing data. The scRNA sequencing data we consider consists of spliced RNA gene counts and RNA velocity, the time derivative of gene counts. DGP-LVM allows inclusion of both these information into a single model (see Section 3.1). Since the RNA velocity is not an exact derivative of spliced RNA counts, it induces a scale difference that is solved by DGP-LVM as shown in Section 3.1.1. Given that single-cell RNA sequencing data is multi-dimensional, DGP-LVM is designed as a multi-output model (see Section 3.2). The primary aim of DGP-LVM is to estimate the latent inputs as explained in Section 3.3, which perfectly aligns with pseudotime estimation since pseudotime is an unobserved cell ordering, hence is considered as a latent variable. Moreover, the RNA sequencing data comes with its own cell capture time or experimental time which can be considered as a noisy version of the true pseudotime.

3.5 Bayesian inference

We estimate DGP-LVMs in a Bayesian framework using MCMC sampling. In DGP-LVM, the parameters of interest are the latent inputs x with the data being y and y' and the set of covariance function hyperparameters denoted by θ . Following from the specification in (10), the joint probability density factorizes as

$$p(y, y', x, \theta) = p(y | x, \theta) p(y' | x, \theta) p(x) p(\theta). \quad (14)$$

where $p(y | x, \theta)$ and $p(y' | x, \theta)$ denote the respective GP-based likelihoods, $p(x)$ denotes the prior for the latent x implied by the measurement model (13), and $p(\theta)$ denotes priors for the covariance function hyperparameters. More details on the choice of prior distributions are discussed in Section 4.2. Using Bayes' rule, we obtain the joint posterior over x and θ as

$$p(x, \theta | y, y') = \frac{p(y | x, \theta) p(y' | x, \theta) p(x) p(\theta)}{\int \int p(y | x, \theta) p(y' | x, \theta) p(x) p(\theta) dx d\theta}. \quad (15)$$

Posterior samples of x and θ are obtained through MCMC sampling via extensions of Hamiltonian Monte Carlo (Neal, 2011; Hoffman and Gelman, 2014). We implemented all models in Stan using the RStan interface (Stan Development Team, 2024).

4 Simulation study

The fundamental issue for validating and comparing models designed to estimate latent variables is the lack of ground truth values for real-world data. Thus, it is crucial to test any latent variable model through extensive simulations where the ground truth is available and controllable. Below, we discuss and provide evidence for the importance of our proposed model innovations. Concretely, we showcase DGP-LVM on multiple simulated data setups that closely represent the complexities of a real scRNA sequencing data.

4.1 Simulated data

We consider two scenarios to generate simulated data. In our first scenario, we generate data from a multi-output GP with scaled derivative SE covariance function with varying hyperparameters and correlated outputs (see Section 3). This constitutes the case where DGP-LVMs align with the underlying process. However, datasets generated this way can vary strongly in the amount of signal they contain, thus adding a lot of random variation in the simulation results. To account for this issue, in our second scenario, we generate data from a derivative periodic process with the true generating function

$$f_{ij} = \alpha_j \sin\left(\frac{x_i}{\rho_j}\right) \quad \text{and} \quad f'_{ij} = \frac{\alpha'_j}{\rho_j} \cos\left(\frac{x_i}{\rho_j}\right) \quad (16)$$

and corresponding data simulations

$$y_{ij} \sim \mathcal{N}(f_{ij}, \sigma^2) \quad \text{and} \quad y'_{ij} \sim \mathcal{N}(f'_{ij}, \sigma'^2). \quad (17)$$

The hyperparameters of this data generating process fulfill a similar purpose than those of SE derivative GPs, hence we choose to use the same hyperparameter names for simplicity. This second scenario is important on two counts. First, it allows us to better control the amount of signal contained in each generated dataset. Second, it demonstrates that DGP-LVM can achieve good results even when the underlying generating process is not actually a GP.

To demonstrate the adversity of scale difference between y and y' , we induce a scaling factor of $\lambda = 3$ that propagates through the GP marginal SD and error SD (see Section 3.1.1).

The GP marginal SD for the output y and the derivative y' are related through λ such that $\alpha = \lambda\alpha'$. Similarly for the error SD, $\sigma = \lambda\sigma'$. Therefore, we only specify sampling distributions for $\alpha' \sim \text{Uniform}(0.4, 0.6)$ and $\sigma' \sim \text{Uniform}(0.05, 0.15)$. The ground truth GP length scale is sampled as $\rho \sim \text{Uniform}(0.5, 1)$. The choice of our sampling distributions enabled us to explicitly select a range of values for our hyperparameters for which the simulated GP data would contain enough signals. In reality, $\lambda > 3$ or $\lambda < 1/3$ may very well occur (see Section 5). In the simulations, we chose to avoid more extreme λ values to prevent substantial convergence issues for models without scaling modifications. This allows us to showcase these models' (reduced) performance without confounding this finding with convergence considerations. Further, we introduce an uniform between-dimension correlation of 0.5 for the simulated GP scenario as to represent moderate interactions between outputs. Combined with the sampling of true hyperparameters for each output dimension, our simulated data mimics the real-world data scenario where such assumptions are prevalent.

Lastly, we generate ground truth for x as a sequence of values between $\{0.5, 10\}$ with equidistant steps of 0.5 and we choose a value for prior measurement SD of the noisy \tilde{x} as $s = 0.3$ (see Section 3.3). This resembles the realistic scenario where observed times are already a relatively good measure of latent pseudotime considering the overall input scale. Both simulation studies are generated as multi-output data with three sets of output dimensions namely $D = 5, 10$ and 20 .

To keep model estimation times within manageable bounds, each simulated dataset contains only 20 observed and 20 derivative sample points. We perform 50 trials per simulation scenario, that is, generate 50 datasets for the GP and the periodic scenario, respectively.

4.2 Model setup

The models within our DGP-LVM framework can vary specifically in four components, namely the inclusion of (1) derivative information, (2) scaled derivatives, (3) varying hyperparameters, as well as (4) correlations across output dimensions. In order to study the individual importance of the four components, we systematically enable/disable each of them and investigate the resulting models' performances. The underlying data generating process contains all of the above components, so any model that only has a subset of components will be misspecified at least to some degree. In our simulations, component combinations were fully crossed where sensible (see Table 1 for an overview). We fit 12 GP models for each selected number of output dimensions D resulting in a total of 36 models fitted per generated dataset for a specific simulation scenario. We only exclude specific, non-sensible combinations. For example, it does not make sense to ask if a GP model, which does not include derivative information, accounts for the scaling of the derivatives. Due to substantial computation requirements of such simulation studies, we only considered models with SE covariance functions. Other Matern kernels (specifically Matern $3/2$) are applied in the case study in Section 5.

We use weakly-informative priors for all GP hyperparameters. For this purpose, we scale the priors of the marginal and error SD parameters (α , σ and their derivative counterparts α' , σ') by the empirical standard deviations of the data denoted by s_y and $s_{y'}$ such that they follow $\text{Normal}(0, s_y)$ and $\text{Normal}(0, s_{y'})$ respectively. This is a common technique used to obtain weakly-informative priors for scale parameters (Bürkner, 2017). The prior on the length scale $\rho \sim \text{InvGamma}(5, 5)$ is roughly based on the mean Euclidean distance between the \tilde{x}_i (as in Section 3.3). As prior for the between-output correlation matrix C , we apply an unimodal LKJ(3) distribution (Lewandowski et al., 2009) defined over the positive definite symmetric matrices with unit diagonals. This distribution is a common prior choice for correlation matrices.

All models were specified in Stan (Stan Development Team, 2024) and fitted with a single MCMC chain of 3000 iterations in total with 1000 warm-ups. We decided to run only a single

Table 1: GP models along with their specifications used for simulated scenarios

Derivative information	Scaled derivatives	Varying hyperparameters	Correlated outputs
✓	✓	✓	✓
✓	✓	✓	✗
✓	✓	✗	✓
✓	✗	✓	✓
✓	✓	✗	✗
✓	✗	✗	✓
✓	✗	✓	✗
✓	✗	✗	✗
✗	✗	✓	✓
✗	✗	✓	✗
✗	✗	✗	✓
✗	✗	✗	✗

Note: Each table row denotes the assigned modifications to the fitted models. The first row shows the modifications involved in DGP-LVM.

chain per model to reduce overall computation times. All models were fitted on all generated datasets. The full study design is depicted in Figure 1.

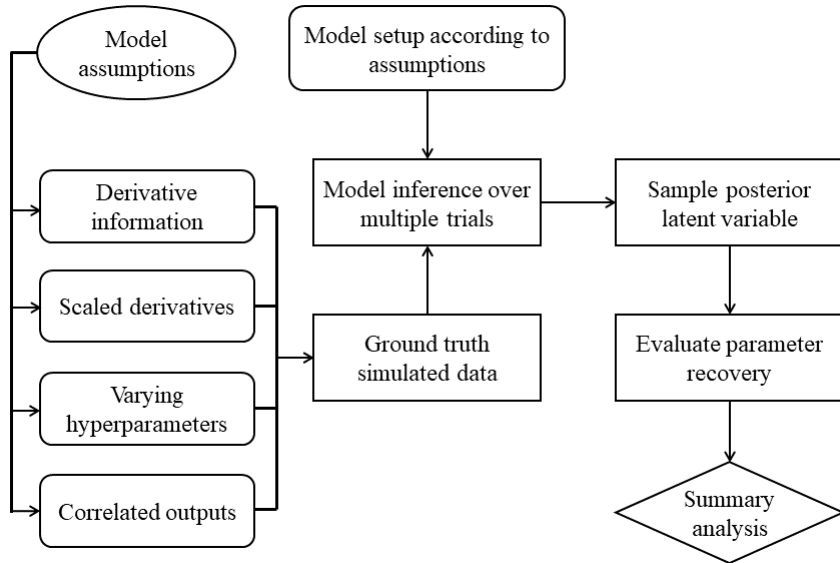


Figure 1: High-level overview of the simulation study design.

4.3 Summary methods

In order to evaluate how well fitted models recover the latent ground truth, we compare posterior samples of the latent input variable x denoted by x_{post} with their respective ground truth values denoted by x_{true} using the root mean squared error (RMSE):

$$\text{RMSE}(x_{post}) = \sqrt{\mathbb{E}(x_{post} - x_{true})^2} \quad (18)$$

where the expectation is taken over the posterior (approximated via samples). $\mathbb{E}(x_{post} - x_{true})^2$ can be decomposed into $\text{Var}(x_{post})$ and $\text{Bias}(x_{post}, x_{true})^2$, thus measuring Bias-variance trade-off. We compute RMSE from all fitted models shown in Table 1 for each set of output dimensions

(5, 10 and 20). We prefer models that provide both low bias indicating posterior mean estimates close to the ground truth as well as lower posterior variance indicating high precision, together resulting in an overall low RMSE.

To analyse RMSE values, we use a multilevel analysis of variance model (ANOVA) fitted with brms (Bürkner, 2017), which disentangles the contributions of each model component. Using a multilevel model is important to account for the dependency between results of all models fitted on the same dataset. We model fixed main effects of scaled derivatives, varying hyperparameters, correlated outputs and number of output dimensions. For this purpose, we consider scaled derivatives as a factor variable with three levels corresponding to models that (a) do not include derivative information, (b) models that include derivative information with scaling and (c) models that include derivative information without scaling. Varying hyperparameters are represented by a binary factor variable that denotes varying vs. constant hyperparameters across output dimensions. Similarly, correlated outputs represented by a binary factor variable that indicates if the multiple outputs are assumed to be correlated or not. We additionally model fixed interaction effects between (a) scaled derivatives and varying hyperparameters and (b) scaled derivatives and correlated outputs. Since our simulation study is performed over 5, 10, and 20 output dimensions, we include dimension as factor variable with three levels and allowed it to interact with all previously mentioned (fixed) main and interaction effects. We account for the dependency structure in the RMSE values, induced by fitting multiple models to the same simulated dataset, by a random intercept over datasets as well as corresponding random slopes of the scaled derivatives, varying hyperparameters, and correlated outputs factors. Further, we account for the dependency in the RMSE values for the 20 latent inputs estimated from a single model through a random intercept per fitted model.

4.4 Model convergence

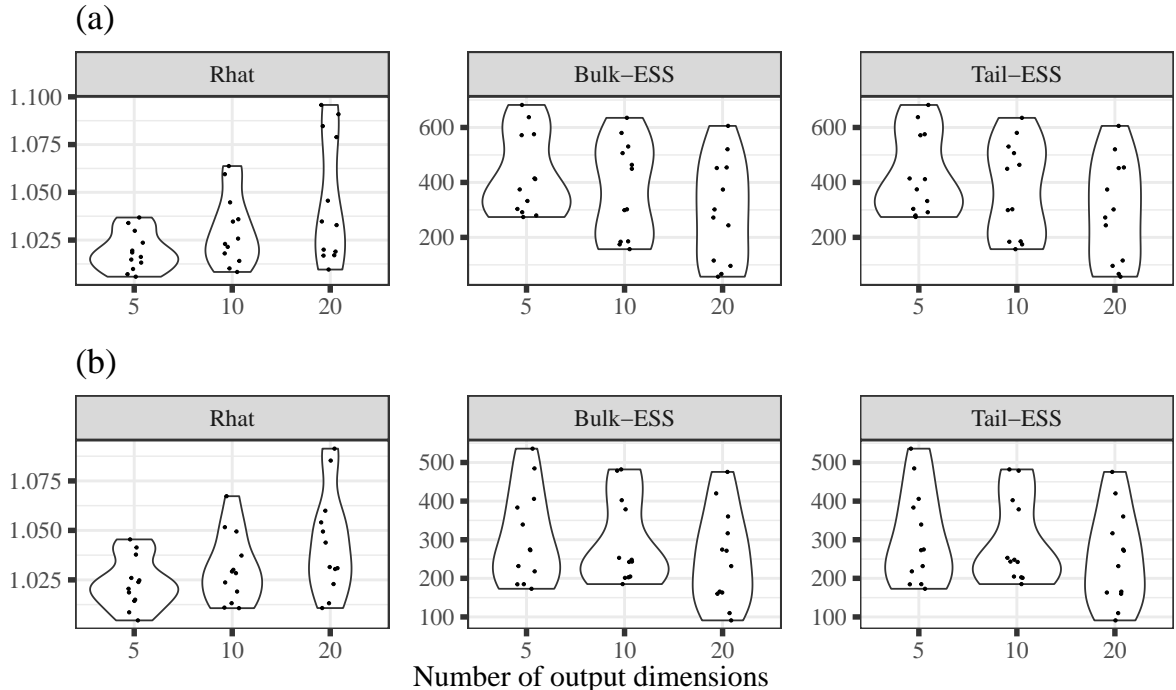


Figure 2: Validation measures for (a) latent inputs and (b) GP hyperparameters for the simulated GP scenario. The individual points correspond to each fitted models.

We investigate the convergence of our fitted GP models using standard MCMC sampling diag-

nostics including state-of-the art versions of the scale-reduction factor \widehat{R} , bulk effective sample size (Bulk-ESS) and tail effective sample size (Tail-ESS) (Vehtari et al., 2021). The combined check of these measures provides a comprehensive picture of individual parameters’ model convergence. In general, \widehat{R} should be very close to 1 and should ideally not exceed 1.01 (Vehtari

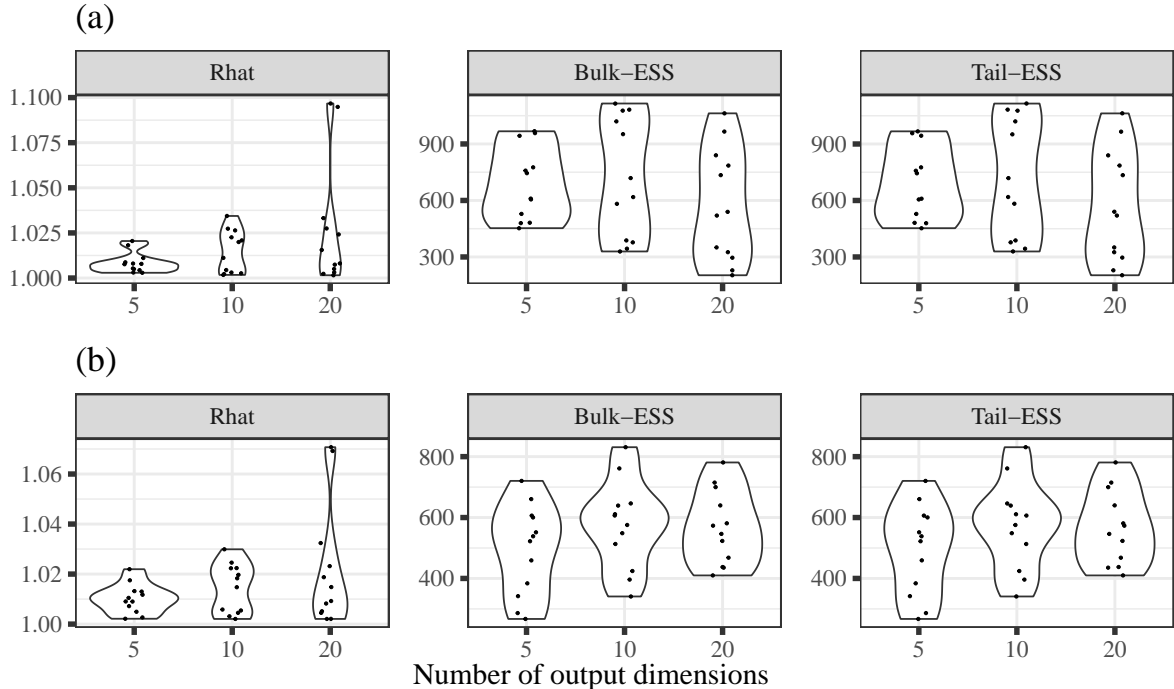


Figure 3: Validation measures for (a) latent inputs and (b) GP hyperparameters for the simulated periodic scenario. The individual points correspond to each fitted models.

et al., 2021). In a simulation setup, we can evaluate the goodness of the posterior estimation also independently of convergence, as we have access to ground truth values. Hence, also in light of the relatively short MCMC chains, we decide to apply a more relaxed threshold of 1.1. Bulk-ESS indicates the reliability of measures of central tendency such as the posterior mean or median. Tail-ESS indicates the reliability of the 5% and 95% quantile estimates, which are commonly used to construct credible intervals. Both Bulk-ESS and Tail-ESS should have values higher than 100 times the number of MCMC chains. We computed all convergence measures with the posterior package (Bürkner et al., 2023).

For both hyperparameters and latent inputs obtained from the simulated GP scenario, we show \widehat{R} , Bulk-ESS, and Tail-ESS in Figure 2. The \widehat{R} were all satisfactory with the exception of a few outlying models fitted on 20-dimensional outputs. Bulk-ESS and Tail-ESS were consistently higher than 100, thus satisfying the recommended criteria. Convergence results were similar for periodic scenario as shown in Figure 3.

4.5 Results

For both GP and periodic simulation scenarios, we evaluated the effects of including derivative information (Figure 4). In addition to the posterior RMSE estimates obtained from the multi-level ANOVA, we also show the prior RMSE that would be expected if we only used the prior measurement model $\tilde{x}_i \sim \mathcal{N}(x_i, s^2)$ to infer x . Accordingly, the prior RMSE acts as a benchmark to illustrate how much precision we gain through the GP modeling of output data. We see how the inclusion of both derivative information and scaling modifications simultaneously results in an overall substantial decrease in mean RMSE thus indicating a better recovery of

the true latent values as compared to models without derivative information. Additionally, the mean RMSE further decreases as we increase the number of output dimensions.

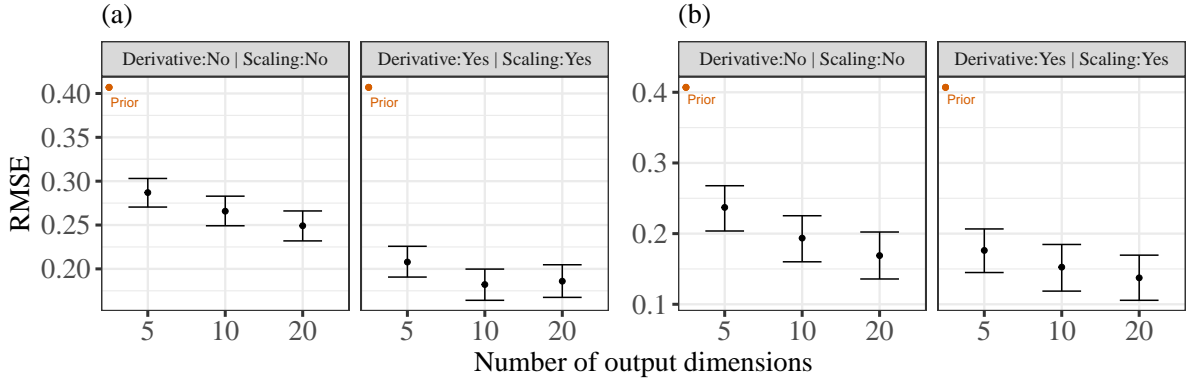


Figure 4: Summarizing main effects of scaled derivatives for simulated (a) GP data and (b) periodic data.

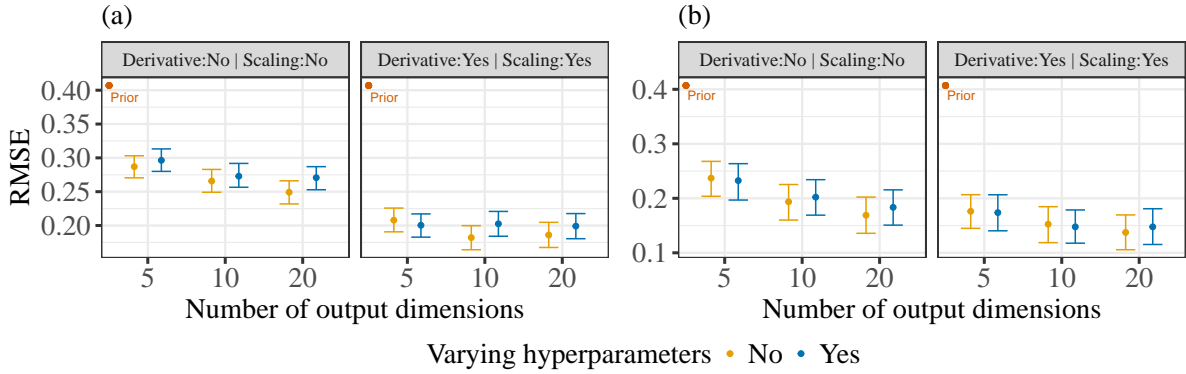


Figure 5: Summarizing interaction effects of scaled derivatives with varying hyperparameters for simulated (a) GP data and (b) periodic data.

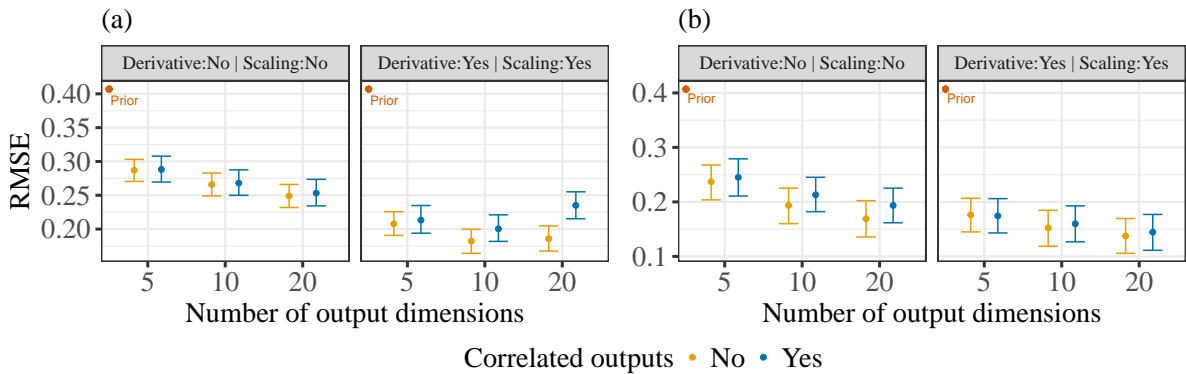


Figure 6: Summarizing interaction effects of scaled derivatives with correlated outputs for simulated (a) GP data and (b) periodic data.

Overall, we see an RMSE reduction of more than 50% compared to the prior RMSE, and a reduction of about 30% compared to the models without derivative information, thus clearly outlining the benefits of using DGP-LVMs. Conversely, when models include derivative information *without* accounting for scale differences, RMSE values are a lot higher, suggesting that the

model performs adversely while estimating latent inputs (Figure 11 in Appendix B). Curiously, the performance of such models is even worse than the models not including derivatives at all, sometimes even worse than when just using the prior measurement model alone. Presumably, this is because hyperparameter estimates are strongly biased if forced to be the same for both regular outputs and their derivatives; at least when the ground truth assumes hyperparameters to be different by a factor of 3 (which is not unrealistic). As an implication, we then also obtain strongly biased latent input estimates, resulting in large RMSEs. This clearly highlights the importance of our derivative covariance function modifications. Without it, using derivative information poses the risk of providing strongly misleading results.

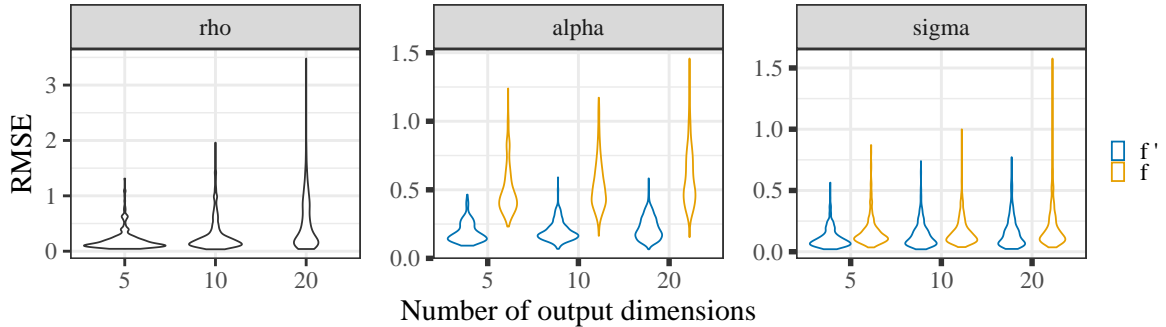


Figure 7: *Hyperparameter RMSEs with respect to their ground truth for the full DGP-LVM including all components. The different colour denotes if the hyperparameters correspond to the original or the derivative part of the model.*

With respect to the other varied components, modeling varying hyperparameters results in a slight increase in RMSE, especially in higher output dimensions (Figure 5). We hypothesize that this is due to the significant increase in the number of estimated parameters, while the amount of data remain constant. Concretely, the number of parameters increase by the number of hyperparameters times the number of output dimensions, which is quite substantial especially for 20 output dimensions. It is likely that, in more data-rich scenarios, modeling hyperparameters as varying over dimensions is strongly beneficial. However, due to the increased computational costs of such a scenario, we do not investigate it in this paper. We see a similar increase in RMSE when modeling outputs as correlated, the reason presumably also being the substantial increase in estimated model parameters. For output dimension D , we estimate $D(D - 1)/2$ number of parameters just for between-dimension correlations. Such a significant increase in parameters becomes visible in the results especially for $D = 20$, as can be seen in Figure 6.

In Figure 7, we show hyperparameter recovery for the full DGP-LVM in the GP simulation scenario. For most of the simulated datasets, the hyperparameters show good recovery as indicated by low RMSE. We do see some extreme RMSE values though, especially for GP length-scale ρ . These extreme cases are explained by the significant increase in the number of estimated parameters, when we consider both varying hyperparameters and correlated outputs without increasing the amount of data. In Figure 8, we show RMSEs when not considering varying hyperparameters or correlated outputs, or both. Clearly, RMSEs are much lower in these cases. We do not display hyperparameter recovery in the periodic simulation scenario as the meaning of true data-generating hyperparameters do not exactly correspond to the hyperparameters of the fitted GP models.

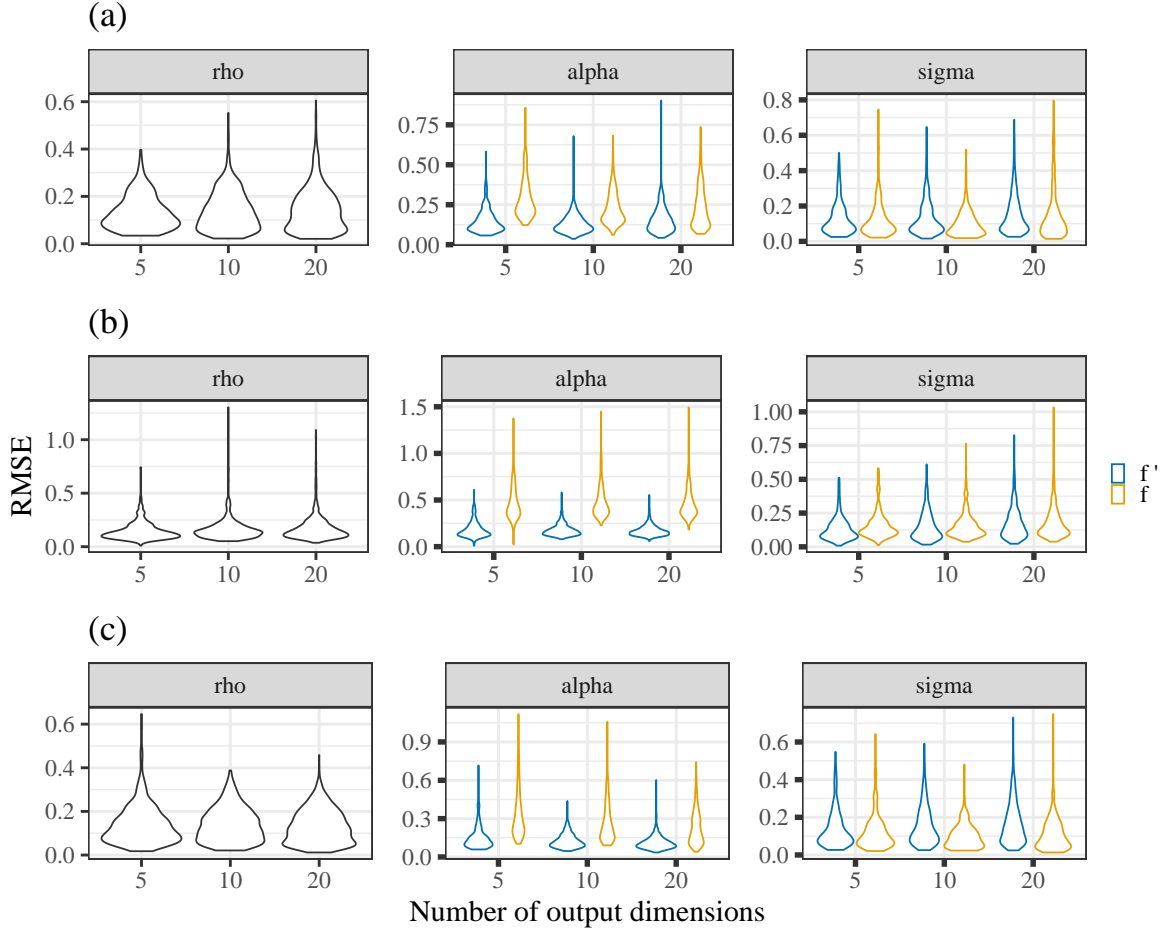


Figure 8: *Hyperparameter RMSEs for models with scaled derivatives (a) without varying hyperparameters, (b) without correlated outputs and (c) without both varying hyperparameters and correlated outputs. The different colour denotes if the hyperparameters correspond to the original or the derivative part of the model.*

5 Case study

In order to showcase the application of DGP-LVM to real-world scRNA sequencing data, we re-analyse cell-cycle data from Mahdessian et al. (2021). This dataset comprises of single-cell RNA expression profiles along the cell cycle as well as corresponding RNA velocities as estimates of expression profile derivatives obtained as a pre-processing step of cytopath, a method for simulation based cell trajectory inference (Gupta et al., 2022). Briefly, we choose this dataset because it covers single-cell transcriptomic profiles of the cell cycle, i.e. a cyclic process going through four phases depicting substantial variation in gene expressions and velocities.

For the purpose of this case study, we use a reduced data set of spliced RNA gene expression data and its corresponding RNA velocity of 20 cells and 12 genes. We sub-sampled the dataset in a stratified fashion so that cells from all four phases are included. We use the experimental time known as "cell hours" in the context of this specific data as the prior \tilde{x} for our latent pseudotime (input) x . Both \tilde{x} and x are real numbers with values ranging between 0 and 1. For our prior measurement SD, we choose $s = 0.03$, so that it is proportional to our choices in simulation studies in Section 4.1.

We fit DGP-LVMs with both our derivative SE and Matern 3/2 covariance functions to showcase the most smooth and the most rough of the common Matern class of covariance functions for

which a derivative version exists. For this case study, we use the same weakly informative prior distributions as our simulation study for the GP marginal SD and error SD parameters. For ρ we use a $\text{InvGamma}(5, 0.5)$ for the SE and $\text{InvGamma}(5, 14)$ for the Matern 3/2 as our GP length scale prior. We these ρ priors, we attempt to account for the varying functional smoothness due to the choice of the covariance function.

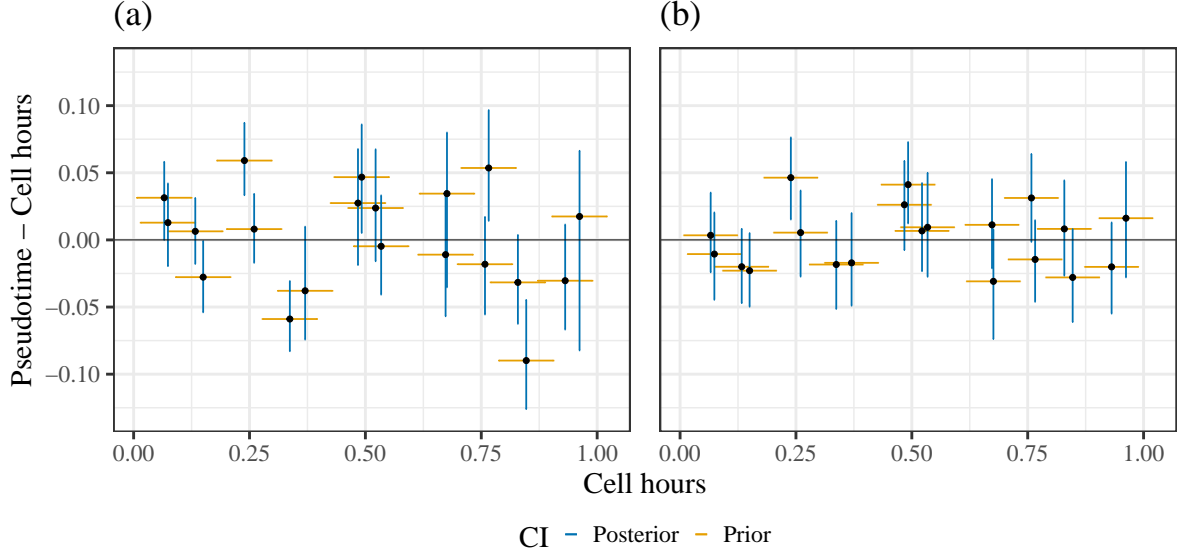


Figure 9: *Difference of latent pseudotime estimates obtained via DGP-LVM with (a) SE and (b) Matern 3/2 covariance functions and prior cell hours. The point ranges horizontally show 95% prior CIs and vertically show 95% posterior CIs. Notice that the posterior CIs are actually much smaller than the prior CIs since y-axis scale is significantly smaller than x-axis.*

As in any real-world latent variable estimation problem, we lack the ground truth to compare the estimated latent values against. Therefore, we study the deviation of the posterior estimates of pseudotime from the cell hours (our prior) by considering the difference or shift in values of the estimated pseudotime from the observed cell hours. The results are shown in Figure 9 with cell hours (prior) on the x-axis and shift (difference of pseudotime and cell hours) on the y-axis. Deviations from the $y = 0$ line indicate that latent pseudotimes are different from their cell hours (prior) as a result of learning from gene expression data and velocities. For some cells, prior-posterior differences are up to 5% of the total time scale. Further, we see that the posterior uncertainties (error bars in y-direction) are substantially smaller (considering the scale of the y-axis compared to x-axis) than the corresponding prior uncertainties (error bars in x-direction), which also indicates that model learning has taken place.

In Figure 10, we show the posterior distributions of GP hyperparameters. We see strongly varying length-scales ρ , marginal SDs α and error SDs σ across different genes (output dimensions) for both SE and Matern 3/2 models. This clearly points to the necessity of modeling hyperparameters as varying across genes. We also see significant scale differences between the marginal SDs α and α' corresponding to gene expression and velocity outputs, respectively. Similar results are seen for the error SDs σ and σ' . These results indicate significant scale differences between output RNA gene expression and its derivative RNA velocity. Interestingly, the scale differences go in both directions, such that for some genes $\alpha > \alpha'$ and for others $\alpha < \alpha'$. While the direction is not important for the DGP-LVM models, it may be highly relevant for understanding the biological processes in which the specific genes are involved.

That said, this case study is meant only as a simple example for demonstrating the application

of DGP-LVMs on real-world data. We would like to caution against any specific biological interpretation of the results at this point.

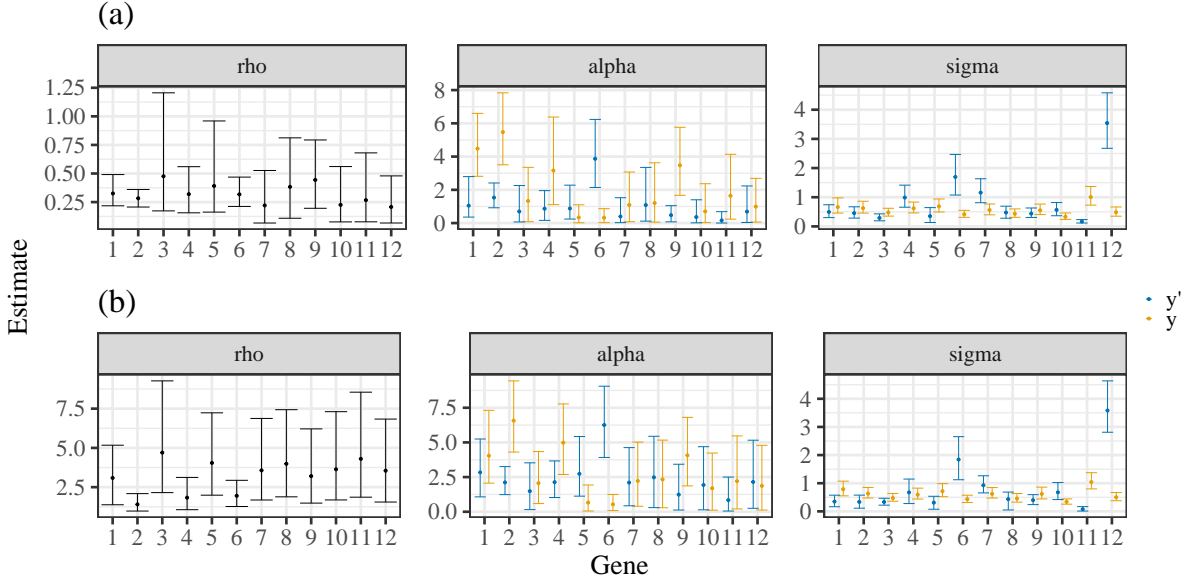


Figure 10: *Hyperparameters for DGP-LVM with (a) SE and (b) Matern 3/2 covariance functions. The points indicate posterior mean and the point ranges indicate 95% CIs for each hyperparameter per output dimension. The different colours denote correspondence to the output y or its derivative y' .*

6 Discussion

Motivated by a real-world problem in the area of single-cell biology, we developed a general statistical modeling framework based on derivative Gaussian processes. In the real-world case, we aim at estimating the latent ordering of cells from RNA gene expression levels and its corresponding time derivative RNA velocity. For this purpose, we developed DGP-LVM, a derivative GP latent variable model that includes derivative information in a multi-output probabilistic framework while accounting for significant scale differences between the outputs and their derivatives. Moreover, it allows the parameters of the model to learn varying information from multiple outputs, which is important in case of scRNA sequencing data where the outputs are different genes, thus accounting for gene-specific information. The model also accounts for between-output correlations since the genes are known to interact with each other. In our extensive simulation studies, we provide clear evidence for the importance of our proposed covariance function modifications. While we specifically focused on modifying the SE and Matern class of covariance functions, our framework is generally applicable for any choice of covariance function that is twice differentiable.

This paper is only the first step towards tackling latent input estimation with derivative Gaussian processes. The current main limitation of DGP-LVMs is their data-scalability as they cannot be easily applied to large amounts of data, such as full sized scRNA sequencing datasets, yet. For a dataset of size N , exact GPs have a complexity of $O(N^3)$ in operations and $O(N^2)$ in memory. In case of multi-output GPs with correlated outputs and varying hyperparameters, the complexities increase to $O(N^3D^3)$ and $O(N^2D^2)$ respectively, where D is the number of output dimensions (Hensman et al., 2013a). Additionally, when performing Bayesian inference via HMC involving a total of T unnormalized log posterior evaluations, the number of operations increases to even $O(N^3D^3T)$. Together, this limits inference for exact GPs on data

with large N or D . From a real-world data point of view, scRNA sequencing data frequently has a few thousand cells (sample size N) with number of genes (output dimensions D) in the high hundreds after standard pre-processing steps. In case of DGP-LVM, this issue is even more severe due to adding derivative information, effectively doubling the sample size N . To address the computational limitations of DGP-LVM in terms of data-scalability, future research should consider extending approximate GP approaches (e.g., Riutort-Mayol et al., 2022) to our DGP-LVM framework.

Another aspect for future research is the choice of prior distributions. Here, we focused on weakly-informative priors for the GP hyperparameters in both our simulation studies and the real-world case study. That said, DGP-LVMs will likely benefit from using stronger priors informed by the application-specific subject matter knowledge, specifically in data-sparse scenarios. This not only applies to priors for the GP hyperparameters, but also to the priors of the latent input variables. The combination of scalable approximations along with stronger prior specifications would foster the general applicability of DGP-LVMs and further increase their accuracy of estimating latent variables.

Code availability

The code for the model development, simulation studies as well as the results can be found here: <https://github.com/Soham6298/DGP-LVM>.

References

- Ahmed, S., Rattray, M., and Boukouvalas, A. (2019). GrandPrix: scaling up the Bayesian GPLVM for single-cell data. *Bioinformatics*, 35(1):47–54.
- Bergen, V., Lange, M., Peidli, S., Wolf, F. A., and Theis, F. J. (2020). Generalizing rna velocity to transient cell states through dynamical modeling. *Nature Biotechnology*.
- Bonilla, E. V., Chai, K., and Williams, C. (2007). Multi-task Gaussian Process Prediction. In *Advances in Neural Information Processing Systems*, volume 20. Curran Associates, Inc.
- Buettner, F., Natarajan, K. N., Casale, F. P., Proserpio, V., Scialdone, A., Theis, F. J., Teichmann, S. A., Marioni, J. C., and Stegle, O. (2015). Computational analysis of cell-to-cell heterogeneity in single-cell RNA-sequencing data reveals hidden subpopulations of cells. *Nature Biotechnology*, 33(2):155–160. Number: 2 Publisher: Nature Publishing Group.
- Buettner, F. and Theis, F. J. (2012). A novel approach for resolving differences in single-cell gene expression patterns from zygote to blastocyst. *Bioinformatics*, 28(18):i626–i632.
- Bürkner, P.-C. (2017). brms: An R Package for Bayesian Multilevel Models Using Stan. *Journal of Statistical Software*, 80:1–28.
- Bürkner, P.-C., Gabry, J., Kay, M., and Vehtari, A. (2023). posterior: Tools for working with posterior distributions. R package version 1.5.0.
- Campbell, K. and Yau, C. (2015). Bayesian Gaussian Process Latent Variable Models for pseudotime inference in single-cell RNA-seq data. Pages: 026872 Section: New Results.
- Campbell, K. R. and Yau, C. (2018). A descriptive marker gene approach to single-cell pseudotime inference. *Bioinformatics*, 35(1):28–35.
- Cressie, N. A. C. (1993). *Statistics for Spatial Data*. Wiley, New York.

- Eriksson, D., Dong, K., Lee, E. H., Bindel, D., and Wilson, A. G. (2018). Scaling Gaussian Process Regression with Derivatives. arXiv:1810.12283 [cs, stat].
- Gupta, R., Cerletti, D., Gut, G., Oxenius, A., and Claassen, M. (2022). Simulation-based inference of differentiation trajectories from RNA velocity fields. *Cell Reports Methods*, 2(12):100359.
- Haque, A., Engel, J., Teichmann, S. A., and Lönnberg, T. (2017). A practical guide to single-cell RNA-sequencing for biomedical research and clinical applications. *Genome Medicine*, 9(1):75.
- Hensman, J., Fusi, N., and Lawrence, N. D. (2013a). Gaussian processes for big data. *CoRR*, abs/1309.6835.
- Hensman, J., Lawrence, N. D., and Rattray, M. (2013b). Hierarchical Bayesian modelling of gene expression time series across irregularly sampled replicates and clusters. *BMC Bioinformatics*, 14(1):252.
- Hoffman, D. M. and Gelman, A. (2014). The no-u-turn sampler. *Journal of Machine Learning Research*.
- Joukov, V. and Kulić, D. (2022). Fast Approximate Multioutput Gaussian Processes. *IEEE Intelligent Systems*, 37(4):56–69. Conference Name: IEEE Intelligent Systems.
- La Manno, G., Soldatov, R., Zeisel, A., Braun, E., Hochgerner, H., Petukhov, V., Lidschreiber, K., Kastriiti, M. E., Lönnberg, P., Furlan, A., Fan, J., Borm, L. E., Liu, Z., van Bruggen, D., Guo, J., He, X., Barker, R., Sundström, E., Castelo-Branco, G., Cramer, P., Adameyko, I., Linnarsson, S., and Kharchenko, P. V. (2018). RNA velocity of single cells. *Nature*, 560(7719):494–498.
- Lalchand, V., Ravuri, A., and Lawrence, N. D. (2022). Generalised GPLVM with Stochastic Variational Inference. In *Proceedings of The 25th International Conference on Artificial Intelligence and Statistics*, pages 7841–7864. PMLR. ISSN: 2640-3498.
- Lawrence, N. (2003). Gaussian Process Latent Variable Models for Visualisation of High Dimensional Data. In *Advances in Neural Information Processing Systems*, volume 16. MIT Press.
- Lawrence, N. (2005). Probabilistic non-linear principal component analysis with gaussian process latent variable models. *Journal of Machine Learning Research*, 6(60):1783–1816.
- Lewandowski, D., Kurowicka, D., and Joe, H. (2009). Generating random correlation matrices based on vines and extended onion method. *Journal of Multivariate Analysis*, 100(9):1989–2001.
- Losick, R. and Desplan, C. (2008). Stochasticity and Cell Fate. *Science*, 320(5872):65–68. Publisher: American Association for the Advancement of Science.
- Maamar, H., Raj, A., and Dubnau, D. (2007). Noise in Gene Expression Determines Cell Fate in *Bacillus subtilis*. *Science*, 317(5837):526–529. Publisher: American Association for the Advancement of Science.
- Mahdessian, D., Cesnik, A. J., Gnann, C., Danielsson, F., Stenström, L., Arif, M., Zhang, C., Le, T., Johansson, F., Schutten, R., Bäckström, A., Axelsson, U., Thul, P., Cho, N. H., Carja, O., Uhlén, M., Mardinoglu, A., Stadler, C., Lindskog, C., Ayoglu, B., Leonetti, M. D., Pontén, F., Sullivan, D. P., and Lundberg, E. (2021). Spatiotemporal dissection of the cell cycle with single-cell proteogenomics. *Nature*, 590(7847):649–654. Number: 7847 Publisher: Nature Publishing Group.

- Moreno-Muñoz, P., Artés, A., and Álvarez, M. (2018). Heterogeneous Multi-output Gaussian Process Prediction. In *Advances in Neural Information Processing Systems*, volume 31. Curran Associates, Inc.
- Neal, R. (2011). “MCMC Using Hamiltonian Dynamics.” In *Handbook of Markov Chain Monte Carlo*, edited by Steve Brooks, Andrew Gelman, Galin L. Jones, and Xiao-Li Meng, 116–62. Chapman; Hall/CRC.
- Padidar, M., Zhu, X., Huang, L., Gardner, J., and Bindel, D. (2021). Scaling Gaussian Processes with Derivative Information Using Variational Inference. In *Advances in Neural Information Processing Systems*, volume 34, pages 6442–6453. Curran Associates, Inc.
- Raj, A. and Oudenaarden, A. v. (2008). Nature, Nurture, or Chance: Stochastic Gene Expression and Its Consequences. *Cell*, 135(2):216–226. Publisher: Elsevier.
- Rasmussen, C. E. and Williams, C. K. I. (2006). *Gaussian Processes for Machine Learning*. The MIT Press.
- Reid, J. E. and Wernisch, L. (2016). Pseudotime estimation: deconfounding single cell time series. *Bioinformatics*, 32(19):2973–2980.
- Riutort-Mayol, G., Bürkner, P.-C., Andersen, M. R., Solin, A., and Vehtari, A. (2022). Practical Hilbert space approximate Bayesian Gaussian processes for probabilistic programming. *Statistics and Computing*, 33(1).
- Solak, E., Murray-smith, R., Leithead, W., Leith, D., and Rasmussen, C. (2002). Derivative Observations in Gaussian Process Models of Dynamic Systems. In *Advances in Neural Information Processing Systems*, volume 15. MIT Press.
- Stan Development Team (2024). *Stan Modeling Language Users Guide and Reference Manual*, 2.32.0.
- Teh, Y. W., Seeger, M., and Jordan, M. I. (2005). Semiparametric Latent Factor Models. *Proceedings of Machine Learning Research*.
- Titsias, M. (2009). Variational Learning of Inducing Variables in Sparse Gaussian Processes. In *Proceedings of the Twelfth International Conference on Artificial Intelligence and Statistics*, pages 567–574. PMLR. ISSN: 1938-7228.
- Titsias, M. and Lawrence, N. D. (2010). Bayesian Gaussian Process Latent Variable Model. In *Proceedings of the Thirteenth International Conference on Artificial Intelligence and Statistics*, pages 844–851. JMLR Workshop and Conference Proceedings. ISSN: 1938-7228.
- Trapnell, C., Cacchiarelli, D., Grimsby, J., Pokharel, P., Li, S., Morse, M., Lennon, N. J., Livak, K. J., Mikkelsen, T. S., and Rinn, J. L. (2014). The dynamics and regulators of cell fate decisions are revealed by pseudotemporal ordering of single cells. *Nature Biotechnology*, 32(4):381–386. Number: 4 Publisher: Nature Publishing Group.
- Vehtari, A., Gelman, A., Simpson, D., Carpenter, B., and Bürkner, P.-C. (2021). Rank-Normalization, Folding, and Localization: An Improved \hat{R} for Assessing Convergence of MCMC (with Discussion). *Bayesian Analysis*, 16(2):667 – 718.
- Williams, C. and Rasmussen, C. (1995). Gaussian Processes for Regression. In *Advances in Neural Information Processing Systems*, volume 8. MIT Press.

Appendix

Appendix A: Derivative covariance functions

Proof of the derivative covariance function structure

Lemma: Let $X \in \mathcal{X}$ be a random variable and $g : \mathbb{R} \times \mathcal{X} \rightarrow \mathbb{R}$ is a function $\ni g(t, X)$ is integrable $\forall t$ and g is continuously differentiable w.r.t t . Assume a random variable $Z \ni \left| \frac{\delta}{\delta t} g(t, X) \right| \leq Z$ almost surely $\forall t$ and $E(Z) < \infty$, then $\frac{\delta}{\delta t} E(g(t, X)) = E\left(\frac{\delta}{\delta t} g(t, X)\right)$.

Let us consider y_i and v_j such that $v_j = \frac{\delta y_j}{\delta x_j}$ where we consider a Gaussian Process model with $y = f(x) + \epsilon$. For a GP model $\text{Cov}(y_i, y_j)$ is completely defined using corresponding inputs x_i and x_j by a covariance function. We see that

$$\begin{aligned}
\text{Cov}(y_i, v_j) &= \mathbb{E}((y_i - \mathbb{E}(y_i))(v_j - \mathbb{E}(v_j))) \\
&= \mathbb{E}\left((y_i - \mathbb{E}(y_i))\left(\frac{\delta}{\delta x_j} y_j - \mathbb{E}\left(\frac{\delta}{\delta x_j} y_j\right)\right)\right) \\
&= \mathbb{E}\left((y_i - \mathbb{E}(y_i))\left(\frac{\delta}{\delta x_j} y_j - \frac{\delta}{\delta x_j} (\mathbb{E}(y_j))\right)\right) && \text{(By DCT)} \\
&= \mathbb{E}\left((y_i - \mathbb{E}(y_i)) \frac{\delta}{\delta x_j} (y_j - (\mathbb{E}(y_j)))\right) && \text{(derivative over subtraction)} \\
&= \mathbb{E}\left(\frac{\delta}{\delta x_j} (y_i - \mathbb{E}(y_i)) (y_j - (\mathbb{E}(y_j)))\right) && (y_i\text{'s are constant w.r.t } x_j) \\
&= \frac{\delta}{\delta x_j} (\mathbb{E}((y_i - \mathbb{E}(y_i)) (y_j - (\mathbb{E}(y_j))))) && \text{(By DCT)} \\
&= \frac{\delta}{\delta x_j} \text{Cov}(y_i, y_j).
\end{aligned}$$

Using similar reasoning and with $v_i = \frac{\delta y_i}{\delta x_i}$ and $v_j = \frac{\delta y_j}{\delta x_j}$, we find

$$\begin{aligned}
\text{Cov}(v_i, v_j) &= \mathbb{E}((v_i - \mathbb{E}(v_i))(v_j - \mathbb{E}(v_j))) \\
&= \mathbb{E}\left(\left(\frac{\delta}{\delta x_i} y_i - \mathbb{E}\left(\frac{\delta}{\delta x_i} y_i\right)\right)\left(\frac{\delta}{\delta x_j} y_j - \mathbb{E}\left(\frac{\delta}{\delta x_j} y_j\right)\right)\right) \\
&= \mathbb{E}\left(\left(\frac{\delta}{\delta x_i} y_i - \frac{\delta}{\delta x_i} \mathbb{E}(y_i)\right)\left(\frac{\delta}{\delta x_j} y_j - \frac{\delta}{\delta x_j} \mathbb{E}(y_j)\right)\right) && \text{(By DCT)} \\
&= \mathbb{E}\left(\frac{\delta}{\delta x_i} \left(\frac{\delta}{\delta x_j} (y_i - \mathbb{E}(y_i)) (y_j - \mathbb{E}(y_j))\right)\right) && \text{(derivative over constants)} \\
&= \frac{\delta^2}{\delta x_i \delta x_j} \text{Cov}(y_i, y_j) && \text{(By DCT)}
\end{aligned}$$

Derivative covariance functions

In the following covariance functions, α is GP marginal SD corresponding to output y ; α' is the GP marginal SD corresponding to derivative output y' ; ρ is the GP length scale parameter.

1. Squared Exponential

$$K = \alpha^2 \exp\left(-\frac{(x_i - x_j)^2}{2\rho^2}\right)$$

$$K_{01} = \frac{\delta K}{\delta x_j} = \alpha\alpha' \frac{(x_i - x_j)}{\rho^2} \exp\left(-\frac{(x_i - x_j)^2}{2\rho^2}\right)$$

$$K_{10} = \frac{\delta K}{\delta x_i} = \alpha\alpha' \frac{(x_j - x_i)}{\rho^2} \exp\left(-\frac{(x_i - x_j)^2}{2\rho^2}\right)$$

$$K_{11} = \frac{\delta^2 K}{\delta x_i \delta x_j} = \frac{\alpha'^2}{\rho^4} (\rho^2 - (x_i - x_j)^2) \exp\left(-\frac{(x_i - x_j)^2}{2\rho^2}\right)$$

2. Matern 3/2

$$K = \alpha^2 \left(1 + \frac{\sqrt{3(x_i - x_j)^2}}{\rho}\right) \exp\left(-\frac{\sqrt{3(x_i - x_j)^2}}{\rho}\right)$$

$$K_{01} = \frac{\delta K}{\delta x_j} = \alpha\alpha' \left(\frac{3(x_i - x_j)}{\rho^2}\right) \exp\left(-\frac{\sqrt{3(x_i - x_j)^2}}{\rho}\right)$$

$$K_{10} = \frac{\delta K}{\delta x_i} = \alpha\alpha' \left(\frac{3(x_j - x_i)}{\rho^2}\right) \exp\left(-\frac{\sqrt{3(x_i - x_j)^2}}{\rho}\right)$$

$$K_{11} = \frac{\delta^2 K}{\delta x_i \delta x_j} = \alpha'^2 \left(\frac{3}{\rho^2}\right) \left(1 - \frac{\sqrt{3(x_i - x_j)^2}}{\rho}\right) \exp\left(-\frac{\sqrt{3(x_i - x_j)^2}}{\rho}\right)$$

3. Matern 5/2

$$K = \alpha^2 \left(1 + \frac{\sqrt{5(x_i - x_j)^2}}{\rho} + \frac{5(x_i - x_j)^2}{3\rho^2}\right) \exp\left(-\frac{\sqrt{5(x_i - x_j)^2}}{\rho}\right)$$

$$K_{01} = \frac{\delta K}{\delta x_j} = \alpha\alpha' \left(\frac{5(x_i - x_j)}{3\rho^2}\right) \left(1 + \frac{\sqrt{5(x_i - x_j)^2}}{\rho}\right) \exp\left(-\frac{\sqrt{5(x_i - x_j)^2}}{\rho}\right)$$

$$K_{10} = \frac{\delta K}{\delta x_i} = \alpha\alpha' \left(\frac{5(x_j - x_i)}{3\rho^2}\right) \left(1 + \frac{\sqrt{5(x_i - x_j)^2}}{\rho}\right) \exp\left(-\frac{\sqrt{5(x_i - x_j)^2}}{\rho}\right)$$

$$K_{11} = \frac{\delta^2 K}{\delta x_i \delta x_j} = \alpha'^2 \left(\frac{5}{3\rho^2}\right) \left(1 + \frac{\sqrt{5(x_i - x_j)^2}}{\rho} - \frac{5(x_i - x_j)^2}{\rho^2}\right) \exp\left(-\frac{\sqrt{5(x_i - x_j)^2}}{\rho}\right)$$

Appendix B: Additional simulation results

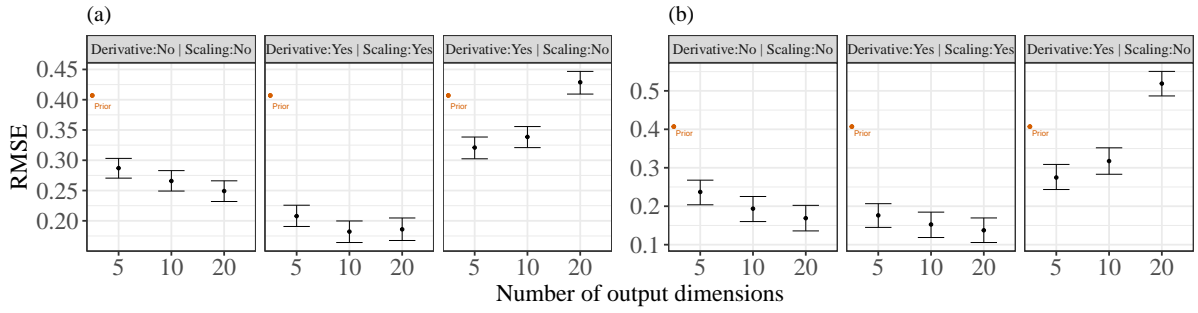


Figure 11: *Summarizing main effects of scaled derivatives for simulated (a) GP data and (b) periodic data for all fitted*

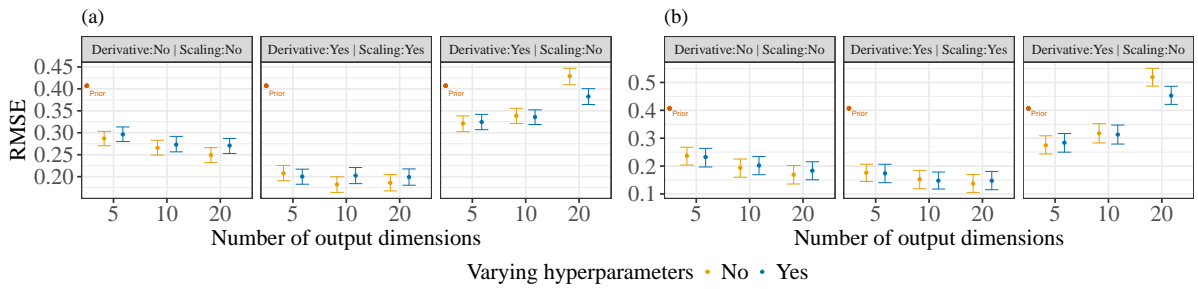


Figure 12: *Summarizing interaction effects of scaled derivatives with varying hyperparameters for simulated (a) GP data and (b) periodic data*

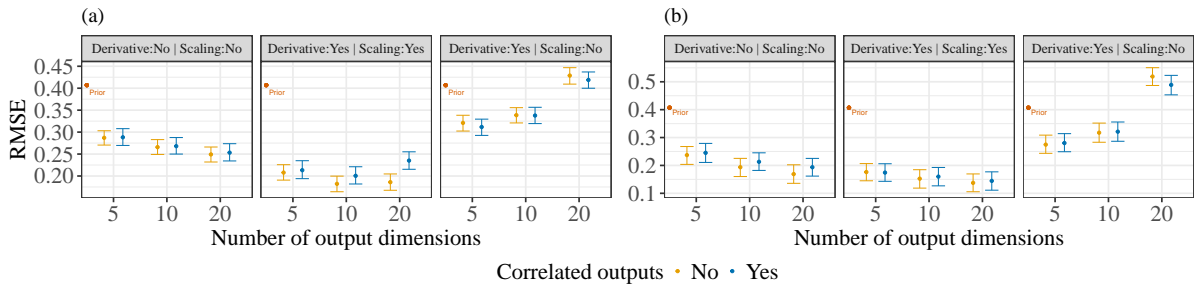


Figure 13: *Summarizing interaction effects of scaled derivatives with correlated outputs for simulated (a) GP data and (b) periodic data*